

1 **Inter-comparison study of atmospheric ^{222}Rn and ^{222}Rn**
2 **progeny monitors**

3 Claudia Grossi^{1,2}, Olivier Llido³, Felix R. Vogel⁴, Victor Kazan³, Alessandro Capuana⁵,
4 Scott D. Chambers⁶, Sylvester Werczynski⁶, Roger Curcoll^{7,8}, Marc Delmotte³, Arturo
5 Vargas¹, Josep-Anton Morguí^{7,9}, Ingeborg Levin⁵, Michel Ramonet³.

6 ¹ Institut de Tècniques Energètiques (INTE), Universitat Politècnica de Catalunya (UPC), Barcelona,
7 Spain;

8 ² Physics Department, Universitat Politècnica de Catalunya (UPC), Barcelona, Spain;

9 ³ Laboratoire des Sciences du Climat et de l'Environnement, Université Paris-Saclay (LSCE/IPSL, CEA-
10 CNRS-UVSQ), Gif-sur-Yvette, France;

11 ⁴ Climate Research Division, Environment and Climate Change Canada, Toronto, Canada;

12 ⁵ Institut für Umweltphysik (IUP), Heidelberg University, Heidelberg, Germany;

13 ⁶ Environmental Research, ANSTO, Lucas Heights, Australia;

14 ⁷ Institut de Ciència i Tecnologia Ambientals (ICTA), Universitat Autònoma de Barcelona (UAB),
15 Cerdanyola del Vallès, Spain;

16 ⁸ Chemical Department, Universitat Politècnica de Catalunya (UPC), Barcelona, Spain;

17 ⁹ Departament Biologia Evolutiva, Ecologia i Ciències Ambientals, Universitat de Barcelona (UB),
18 Barcelona, Spain.

19 *Correspondence to:* Claudia Grossi (Claudia.grossi@upc.edu)

20 **Abstract.**

21 The use of the noble gas radon (^{222}Rn) as tracer for different research studies, for example observation-
22 based estimation of greenhouse gas (GHG) fluxes, has led to the need of high-quality ^{222}Rn activity
23 concentration observations with high spatial and temporal resolution. So far a robust metrology chain for
24 these measurements is not yet available.

25 A portable direct Atmospheric Radon MONitor (ARMON), based on electrostatic collection of ^{218}Po , is
26 nowadays running at Spanish stations. This monitor has not yet been compared with other ^{222}Rn and ^{222}Rn
27 progeny monitors commonly used at atmospheric stations.

28 A 3-month inter-comparison campaign of atmospheric ^{222}Rn and ^{222}Rn progeny monitors based on
29 different measurement techniques was realized during the fall and winter of 2016-2017 to evaluate: i)
30 calibration and correction factors between monitors necessary to harmonize the atmospheric radon

31 observations; and ii) the dependence of each monitor's response in relation to the sampling height,
32 meteorological and atmospheric aerosol conditions.

33 Results of this study have shown that: i) all monitors were able to reproduce the atmospheric radon
34 variability on daily basis; ii) linear regression fits between the monitors exhibited slopes, representing the
35 correction factors, between 0.62 and 1.17 and offsets ranging between -0.85 Bq m^{-3} and -0.23 Bq m^{-3}
36 when sampling 2 m above ground level (a.g.l.). Corresponding results at 100 m a.g.l. exhibited slopes of
37 0.94 and 1.03 with offsets of -0.13 Bq m^{-3} and 0.01 Bq m^{-3} , respectively; iii) no influence of atmospheric
38 temperature and relative humidity on monitor responses was observed for unsaturated conditions at 100 m
39 a.g.l. whereas slight influences (order of 10^{-2}) of ambient temperature were observed at 2 m a.g.l.; iv)
40 changes of the ratio between ^{222}Rn progeny and ^{222}Rn monitor responses were observed under very low
41 atmospheric aerosol concentrations. A more statistically robust evaluation of these last influences based
42 on a longer dataset should be conducted to improve the harmonization of the data. Results also show that
43 the ARMON has a great potential to be used in radon networks. However, its qualities and faults should
44 be deeply investigated in future long-term comparison studies.

45

46 Key words: radon, activity concentration, atmosphere, one-filter, two-filters, electrodeposition

47 1 Introduction

48 Over continents, the natural radioactive noble gas radon (^{222}Rn) (half-life $T_{1/2} = 3.8$ days) is continuously
49 generated within the soil from the decay of radium (^{226}Ra) (Nazaroff and Nero, 1988; Porstendörfer,
50 1994) and it can then escape into the atmosphere by diffusion, depending on soil characteristics and
51 meteorological conditions (Grossi et al., 2011, Lopez-Coto et al., 2013; Karstens et al., 2015). The global
52 ^{222}Rn source into the atmosphere is mainly restricted to land surfaces (Szegváry et al., 2009; Karstens et
53 al., 2015), with the ^{222}Rn flux from water surfaces considered negligible for most applications (Schery
54 and Huang, 2004).

55 In recent decades the atmospheric scientific community has been addressing different research topics
56 using ^{222}Rn as a tracer. Examples of such applications include: the improvement of inverse transport
57 models (Hirao et al., 2010), the improvement of chemical transport models (Jacob and Prather, 1990;
58 Chambers et al. 2019a), the study of atmospheric transport and mixing processes within the planetary
59 boundary layer (Zahorowski et al., 2004; Galmarini, 2006; Baskaran, 2011; Chambers et al., 2011, 2019b;
60 Williams et al., 2011, 2013; Vogel et al. 2013; Vargas et al., 2015; Baskaran, 2016), the experimental
61 estimation of greenhouse gas (GHG) fluxes (Levin et al., 1999; 2011; Vogel et al., 2012; Wada et al.,
62 2013; Grossi et al., 2018), and others listed in Grossi et al. (2016).

63 In light of this, atmospheric ^{222}Rn measurements are being carried out at numerous monitoring stations of
64 GHG concentrations and air quality using three fundamentally different measurement principles: one
65 filter, two filters, and electrostatic deposition (Stockburger and Sittkus, 1966; Polian, 1986; Hopke, 1989;
66 Whittlestone and Zahorowski, 1998; Paatero et al., 1998; Levin et al., 2002). The two most commonly
67 employed measurement systems at European ^{222}Rn monitoring stations are: the dual-flow-loop two-filter

68 monitor (Whittlestone and Zahorowski, 1998; Zahorowski et al. 2004; Chambers et al., 2011, 2014,
69 2018; Griffith et al., 2016), which samples and measures radon directly, and the one-filter monitors, of
70 which several kinds are in use (e.g. Stockburger and Sittkus, 1966; Polian, 1986; Paatero et al., 1998;
71 Levin et al., 2002), which sample and measure aerosol-bound radon progeny. Finally, a third method is
72 being used at several Spanish atmospheric stations (Vargas et al., 2015; Hernández-Ceballos et al., 2015;
73 Grossi et al., 2016; Frank et al., 2016; Grossi et al., 2018; Gutiérrez-Álvarez et al., 2019). This type of
74 instrument performs a direct measurement of ^{222}Rn and ^{220}Rn (thoron) activity concentrations using the
75 already existent method based on the electrostatic deposition of ^{218}Po and ^{216}Po , respectively (Hopke,
76 1989; Tositti et al., 2002; Grossi et al., 2012).

77 The diversity of these three aforementioned measurement techniques could introduce biases or
78 compatibility issues that would limit the comparability of the results obtained by independent studies and
79 the subsequent application of atmospheric radon data for regional-to-global investigations (e.g.
80 Schmithüsen et al., 2017). Thus, a comparative assessment of all the experimental techniques applied for
81 atmospheric ^{222}Rn activity concentration measurements and a harmonization of their datasets is needed, as
82 suggested by the International Atomic Energy Agency (IAEA, 2012).

83 Xia et al. (2010) carried out a comparison of the response of a dual-flow-loop two-filter detector from the
84 Australian Nuclear Science and Technology Organisation (ANSTO, Whittlestone and Zahorowski 1998)
85 and a one-filter monitor (α/β Monitor P3) manufactured by the Bundesamt für Strahlenschutz, Germany
86 (BfS) (Stockburger and Sittkus, 1966), for atmospheric ^{222}Rn measurements under various meteorological
87 conditions at 2.5 m above ground level (a.g.l.) over one year. Their results showed that both systems
88 followed the same patterns and produced very similar results most of the time, except under specific
89 meteorological conditions such as when precipitation or the proximity of the forest canopy could remove
90 short-lived progeny from the air mass to be measured by the one-filter monitor. However, Xia et al.
91 (2010) did not find a clear relationship between precipitation intensity and the ratio between progeny-
92 derived ^{222}Rn and ^{222}Rn activity concentration to convert the progeny signal to ^{222}Rn activity
93 concentration.

94 Grossi et al. (2016) presented results from two short (about 7-9 days) comparisons between a one-filter
95 monitor from Heidelberg University (HRM; Levin et al., 2002), and an Atmospheric Radon MONitor
96 (ARMON, Grossi et al., 2012), an electrostatic deposition monitor from the Universitat Politecnica de
97 Catalunya (UPC). The two comparison campaigns were carried out at a coastal and a mountain site, with
98 sampling in both cases from 10 m a.g.l. These comparisons revealed that the responses of both monitors
99 were in agreement except for water saturated atmospheric conditions or periods of rainfall. Again, the
100 quantity of comparison data was not sufficient to confirm any statistical correlation.

101 Loss of aerosols in the air intake systems can also complicate the derivation of ^{222}Rn activity
102 concentrations from one-filter systems such as the HRM. Levin et al. (2017) carried out an assessment of
103 ^{222}Rn progeny loss in long tubing by laboratory and field experiments. Results of these experiments, for
104 8.2 mm inner diameter (ID) Decabon tubing, gave an empirical correction function for ^{222}Rn progeny
105 measurements, which enables the correction of measurements for this specific experimental setup (e.g.
106 tubing type and diameter, flow rate, aerosol size distribution).

107 Finally, Schmithüsen et al. (2017) conducted an extensive European-wide $^{222}\text{Rn}/^{222}\text{Rn}$ progeny
108 comparison study in order to evaluate the comparative performance of one-filter and two-filter
109 measurement systems, determining potential systematic biases between them, and estimating correction
110 factors that could be applied to harmonize ^{222}Rn activity concentration estimates for their use as a tracer
111 in various atmospheric applications. In this case, the authors employed a HRM monitor as the reference
112 device. It was taken to nine European measurement stations to run for at least one month at each of them.
113 This monitor was run in parallel to other one-filter and two-filter radon monitors operating at each station
114 of interest.

115 Although several inter-comparison campaigns have been carried out in the past, none of them has
116 included simultaneous observations from one-filter, two-filter and electrostatic deposition methods. Here,
117 we present the results of a three-month inter-comparison campaign carried out in the fall and winter of
118 2016-2017 in Gif Sur Yvette (France) where, for the first time, co-located measurements from monitors
119 based on the three measurement principles were included. Two two-filter ^{222}Rn monitors, two single-filter
120 ^{222}Rn progeny monitors and an electrodeposition monitor were run simultaneously under different
121 meteorological and aerosol conditions sampling from heights of 2 and 100 m a.g.l.

122 The main objectives of the present study were to: i) compare the calibration and correction factors
123 between all monitors required to derive harmonized atmospheric radon activity concentrations; and ii)
124 analyze the influence that meteorological and environmental parameters, as well as sampling height, can
125 have on the finally determined ^{222}Rn activity concentration.

126 In the present manuscript the applied methodology is reported, including a short presentation of the ^{222}Rn
127 $/^{222}\text{Rn}$ progeny monitors participating in the campaigns, the sampling sites and the statistical analysis
128 carried out. Finally, the outcomes of the present study are discussed and compared with the ones from
129 Schmithüsen et al. (2017).

130 **2 Methods**

131 In section 2.1 a short description is given of the monitors compared in the experiment, mainly focusing on
132 measurement techniques, instrument calibration and maintenance. The main characteristics of these
133 monitors are then summarized in Table 1. Section 2.2 presents the French atmospheric stations of Orme
134 de Mérissiers (ODM) and Saclay (SAC) where the two phases of the inter-comparison campaign were
135 realized. Section 2.3 briefly describes the devices used to measure the environmental parameters and the
136 atmospheric aerosol concentration at the above sites during the experiments. Finally, the statistical
137 analysis applied is described in section 2.4.

138 **2.1 ^{222}Rn and ^{222}Rn progeny monitors**

139 **2.1.1 Direct methods**

140 **Dual-flow-loop two-filter detectors**

141 The two 1500 L dual-flow-loop two-filter detectors included in this exercise were designed and built at
142 the Australian Nuclear Science and Technology Organisation (ANSTO). This model of detector, which

143 will henceforth be named ANSTO, is based on a previous design by Thomas and Leclare (1970), with
144 some early iterations of the modified design being described by Whittlestone and Zahorowski (1998) and
145 Brunke et al. (2002). The subsequent evolution of two-filter detectors in recent decades, and the current
146 principle of operation, has been described in detail by Williams and Chambers (2016) and Griffiths et al.
147 (2016).

148 During the measurement campaign ambient air was sampled continuously at a rate of 83 L min^{-1} through
149 a 50 mm ID HDPE inlet tube and a 400 L delay volume to allow decay of the short-lived ^{220}Rn ($T_{1/2} = 56$
150 s). The air stream then passes through the first filter, which removes all ambient aerosols as well as ^{222}Rn
151 and ^{220}Rn progeny. The filtered sample, now containing only aerosol-free air and ^{222}Rn gas, enters the
152 main delay volume (1500 L) where ^{222}Rn decay produces new progeny. The newly formed ^{218}Po and
153 ^{214}Po are then collected on a second filter and their subsequent α decays are counted with a ZnS
154 photomultiplier system. Atmospheric ^{222}Rn activity concentrations are then calculated from the α count
155 rate and the flow rate through the chamber.

156 The detection limit of two-filter detectors is directly related to the volume of the main delay chamber. The
157 lower limit of detection of the 1500 L model used in this study was around 0.03 Bq m^{-3} . Under normal
158 operation ANSTO monitors are automatically calibrated in situ every month by injecting radon into the
159 sampling air stream from a well-characterized Pylon ^{226}Ra source (ca. 41 kBq radium at SAC station) for
160 5 hours at a fixed flow rate of $\sim 100 \text{ cc min}^{-1}$. Automatic instrumental background checks, each lasting 24
161 hours, are also performed every 3 months to keep track of long-lived ^{210}Pb accumulation on the detectors
162 second filter (which should be changed every 5 years). Based on a calibration source uncertainty of 4%,
163 coefficient of variability of valid monthly calibrations of 2-6%, and a counting uncertainty of around 2%
164 for radon concentrations $\geq 1 \text{ Bq m}^{-3}$, the total measurement of 1500 L ANSTO radon detectors is typically
165 8-12%. The ANSTO monitors have low-maintenance requirements but, due to their dimensions (2.5 – 3m
166 long) it can be challenging to install them at stations with space restrictions. As an alternative to the 1500
167 L detectors, a 700 L model is also available, which is more portable and has a detection limit of around
168 0.04 Bq m^{-3} .

169 Two ANSTO monitors were used during this study. As explained later in the text these monitors are
170 permanently running at SAC and ODM stations. No calibration source was available when the ANSTO
171 monitor was installed at the ODM site, so calibration and background information derived prior to
172 transport have been used.

173 **Electrostatic deposition monitor**

174 The Atmospheric Radon Monitor (ARMON) used in this experiment was designed and built at the Institut
175 de Tècniques Energètiques (INTE) of the UPC. The ARMON is a portable instrument based on
176 electrostatic deposition method, consisting of alpha spectrometry of positive ions of ^{218}Po electrostatically
177 collected on a detector (Hopke, 1989; Pereira and da Silva, 1989; Tositti et al., 2002). The ARMON is
178 described in detail in Grossi et al. (2012).

179 Sampled air with a flow rate between $1\text{-}2 \text{ L min}^{-1}$, is first filtered to remove ambient ^{222}Rn and ^{220}Rn
180 progeny and then pumped through a $\sim 20 \text{ L}$ spherical detection volume uniformly covered internally with

silver. Within this volume the newly formed ^{222}Rn and ^{220}Rn progeny, i.e. positive ^{218}Po and ^{216}Po ions, respectively, are electrostatically collected on a Passivated Implanted Planar Silicon (PIPS) detector surface by an electrostatic field inside the spherical volume. An 8 kV potential is applied between the PIPS detector base and the sphere walls. As for the ANSTO detector, the sensitivity of this instrument type depends on the detector volume. The design of the monitor employed in this study allows a minimum detectable activity concentration of about 0.2 Bq m^{-3} (Grossi et al., 2012). The measurement efficiency of the electrodeposition method is reduced due to neutralization of the positive ^{218}Po in recombination with OH^- ions in the sampled air (Hopke, 1989). Consequently, it is necessary to dry the sampled air as much as possible before it enters the detection volume. To this end, a dew point of $< -40^\circ\text{C}$ was maintained at both inter-comparison sites using a cryocooler.

Each ARMON is calibrated at the INTE-UPC ^{222}Rn chamber (Vargas et al., 2004) under different ^{222}Rn and relative humidity conditions (Grossi et al., 2012). The radon chamber of the INTE-UPC is a 20 m^3 installation, which allows control of the exhalation rate ($0\text{--}256 \text{ Bq min}^{-1}$) and the ventilation air flow rate ($0\text{--}100 \text{ L min}^{-1}$). The ^{222}Rn source is a dry powder material containing 2100 kBq ^{226}Ra activity enclosed in the source container (RN-1025 model manufactured by Pylon Electronics). The calibration factor F_{cal} of the ARMON used in this study was of 0.39 counts per minute (cpm) per Bq m^{-3} with an uncertainty of 10% ($k=2$). The correction factor for the humidity influence inside the sphere was of $6.5 \cdot 10^{-5}$ per part per million H_2O (ppm) with a maximum uncertainty of 10% ($k=2$). The total uncertainty of the atmospheric radon activity concentration measured by the ARMON is of about 20% ($k=2$) where it is including the calibration factor F_{cal} , the background due to the presence of ^{212}Po from ^{220}Rn and the humidity correction factor (Grossi et al., 2012; Vargas et al., 2015). Every 1-2 years the progeny filter at the ARMON inlet should be changed. The detection volume of the ARMON is safety isolated because it is located within an external wooden cube of 0.18 m^3 .

2.1.2 Non direct methods

One-filter monitors

One-filter detectors measure the decay rates of aerosol-bound ^{222}Rn progeny directly accumulated by air filtration (Schmithüsen et al., 2017). The ^{222}Rn activity concentration is then calculated assuming a constant disequilibrium factor (F_{eq}) for a given site and sampling height between ^{222}Rn and the measured progeny in the sampled air.

In the present study two monitors based on this method were used. One, named here as HRM, was developed at the Institute of Environmental Physics of Heidelberg University, Germany, and is described in detail by Levin et al. (2002). Rosenfeld (2010) describe the most recent version of this monitor for which the electronics, data acquisition, and evaluation hardware and software were modernized. The HRM measurement is based on α spectrometry of ^{222}Rn daughters attached to atmospheric aerosols collected on a static quartz fiber filter (QMA $\varnothing 47 \text{ mm}$) using a surface barrier detector (Canberra CAM 900 mm^2 active surface). The detection limit of the HRM is about 0.05 Bq m^{-3} at a flow rate of about 20 L min^{-1} with an uncertainty below 20% for atmospheric ^{222}Rn levels above 1 Bq m^{-3} . Since one-filter detectors have no need for any delay chambers but use only a compact filter holder with integrated

219 detector and pre-amplifier, the HRM is a small instrument with high portability. Regarding maintenance
220 requirements, the quartz fiber filter should be changed monthly.

221 During the measurement campaign carried out at the Saclay station, where air samples were collected via
222 a 100m Decabon tubing (see below), the line loss correction of Levin et al. (2017) was applied to all data
223 of the HRM. No loss of aerosol was assumed in the short tubing used at Orme de Mérésiers station. Here
224 we report for both sites ^{214}Po activity concentrations. However, for the 100 m intake height at Saclay we
225 would not expect any disequilibrium, meaning that, based on the results from Schmithüsen et al. (2017),
226 the reported ^{214}Po activity concentrations directly correspond to ^{222}Rn activity concentrations. By contrast,
227 for the 2 m intake height at ODM we expect a $^{214}\text{Po}/^{222}\text{Rn}$ disequilibrium of about 0.85 to 0.9.

228 The second type of one-filter monitor participating in this study was built at the Laboratoire des Sciences
229 du Climat et de l'Environnement, LSCE, France (Polian, 1986; Biraud, 2000; Schmithüsen et al., 2017).
230 Within this manuscript this monitor will be called the LSCE monitor. This monitor uses a moving filter
231 band system, which allows the determination of atmospheric ^{222}Rn activity concentration based on
232 measurements of its progeny ^{218}Po and ^{214}Po . Attached ^{222}Rn progeny are collected on a cellulose filter
233 (Pöllman–Schneider) over a one-hour period at a flow rate of 160 L min^{-1} and after this aerosol sampling
234 period, the loaded filter is moved to the α spectrometry for a one hour measurement period by a
235 scintillator from Harshaw Company and photomultiplier from EMI, Electronics Ltd (Biraud, 2000). The
236 minimum detection activity is about 0.01 Bq m^{-3} with an uncertainty of about 20%.

237 Regarding maintenance on regular basis, the LSCE monitor's filter roll has to be changed every three
238 weeks. Automatic detector background is performed every three weeks and counting efficiency is
239 manually tested with an americium source. The instrument is designed to measure radioactive aerosols a
240 few meters above the ground level. An inlet filter is installed to block black carbon or dirt deposition
241 when the instrument is installed in urban areas as the flow rate drops below $9 \text{ m}^3 \text{ h}^{-1}$. The instrument size
242 is about 25 cm high, 40 cm long and 25 cm deep, and it can be easily deployed at a station.

243

Monitor	Method	α Spectrum	Flow Rate (L min^{-1})	Detection Limit (Bq m^{-3})	Typical uncertainty ($k=2$)	Remote Control	Need of dry air sample	Need of corrections depending on the height of the inlet	Portability Level and monitor size	References
ANSTO	Dual- flow- loop two- filter	No	~83	0.03	8-12%	Yes	No	No	Low ; 1.92 m^3	Whittlestone and Zahorowski (1998) ; Brunke et al. (2002)
ARMON	Electrost atic depositi on	Yes	1-2	~0.2	20%	Yes	Yes	No	Medium; 0.18 m^3	Grossi et al. (2012)

HRM	One-filter	Yes	20	~0.05	15-20%	Yes	No	Yes	High; 0.08 m ³	Levin et al. (2002)
LSCE	One-filter	Yes	160	~0.01	20%	Yes	No	Yes	High; 0.03 m ³	Polian, 1986; Biraud, 2000

244 Table 1. Summary of principal characteristics of the ^{222}Rn and ^{222}Rn progeny monitors compared in the
245 present study.

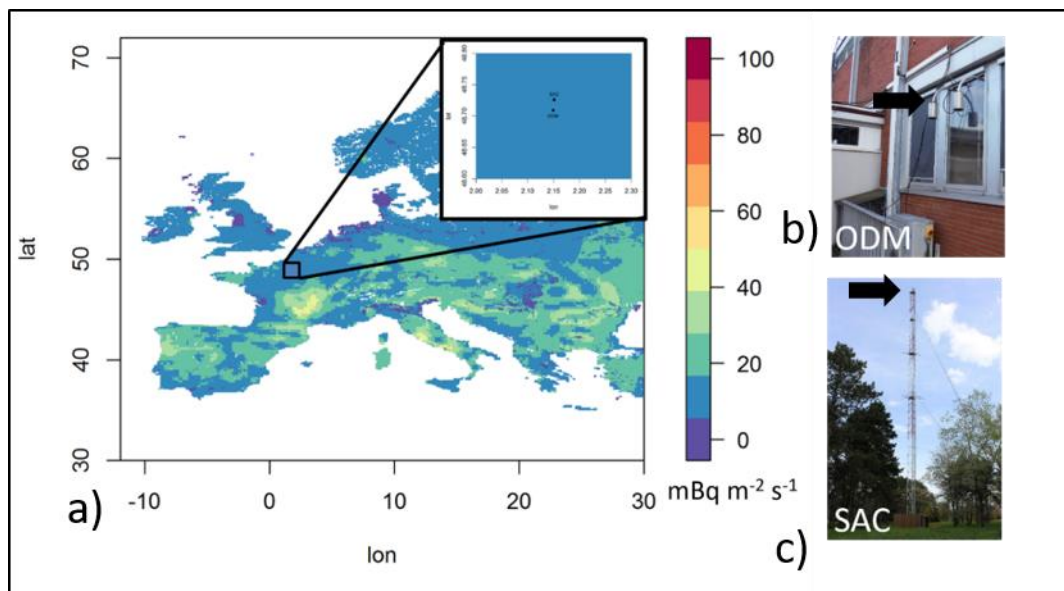
246 **2.2 Sites**

247 The present inter-comparison study was carried out at two stations located 30 km southwest of Paris in
248 the fall and winter of 2016-2017 (Figure 1). Both stations, 3.5 km apart, belong to the LSCE and are
249 located in a region with a radon flux of ca. $5\text{--}10 \text{ mBq m}^{-2} \text{ s}^{-1}$ in winter, according to output of the Karsten
250 et al. (2015) model.

251 Phase I of the measurements started at Orme des Mérisiers (ODM, latitude 48.698, longitude 2.146, 167
252 m above sea level) and ran between 25 November 2016 and 23 January 2017. Here, LSCE and ANSTO
253 (for convenience named here as ANSTO_ODM) monitors are routinely running. During Phase I of the
254 inter-comparison exercise these two monitors were operated in parallel with a HRM and an ARMON.
255 The sampling height for all radon detectors at ODM was 2 m a.g.l.

256 Phase II of the exercise was realized at Saclay (SAC, latitude 48.730, longitude 2.180, Figure 1) between
257 25 January 2017 and 13 February 2017. At this location the sampling inlet height was at 100 m a.g.l. At
258 SAC station another ANSTO monitor (from now on labelled as ANSTO_SAC) was already running. In
259 addition, during Phase II this detector was running in parallel with the portable ARMON and HRM
260 detectors. The LSCE monitor did not participate in Phase II of the experiment.

261 Meteorological parameters were also available at both stations during the inter-comparison periods at
262 heights corresponding to the radon measurements (2 m and 100 m a.g.l.). In the case of the ODM site,
263 atmospheric aerosol concentrations were also measured for this period.



265 Figure 1. The INGOSv2.0 ^{222}Rn flux map (Karstens et al., 2015) is shown for a typical winter month
266 (December), with locations of the ODM and SAC sites shown in inset (a). The radon sampling inlets are
267 indicated both for ODM (b) and SAC (c) by the black arrows.

268 **2.3 Environmental parameters and atmospheric aerosol concentration**

269 Meteorological data used within this study were available from continuous measurements carried out at
270 the SAC and ODM stations at 100 m and at 10 m a.g.l. respectively. The measurements were performed
271 with a Vaisala Weather Transmitter WXT520 (Campbell Scientific) for: (1) wind speed and direction
272 (accuracies of $\pm 3\%$ and $\pm 3\text{ }^{\circ}\text{C}$, respectively); (2) Humidity and temperature (accuracies of $\pm 3\%$ and \pm
273 $0.3\text{ }^{\circ}\text{C}$, respectively). In addition, the atmospheric aerosol concentration was measured at ODM site using
274 a fine dust measurement device Fidas® 200 S (Palas) at 10 m a.g.l.. The measurement range is between 0
275 and 20.000 particles cm^{-3} . All the accuracies refer to the manufacturer's specifications.

276

277 **2.4 Data Analysis**

278 **2.4.1 Correlation factors between monitors**

279 To study the correlation between responses of the different detectors, linear regression models were
280 calculated using hourly atmospheric radon activity concentrations from each monitor. The linear
281 regression fits were calculated following Krystek and Anton (2007), relative to the two portable detectors,
282 ARMON and HRM, because they both were measuring at SAC and at ODM.

283 **2.4.2 Analysis of the influence of the environmental and meteorological parameters on detector
284 response**

285 The present study intended to build upon the findings of Xia et al. (2010) and Schmithüsen et al., (2017)
286 regarding the possible influence of meteorological conditions on the response of radon and radon progeny
287 monitors.

288 With this in mind, the ratio between hourly atmospheric ^{222}Rn activity concentrations measured and/or
289 obtained by the HRM, LSCE and ANSTO monitors, and that measured by the ARMON were calculated,
290 and their variability analyzed in relation to hourly atmospheric temperature, relative humidity and
291 atmospheric aerosol concentration measured at ODM and at SAC, respectively. Not enough rain data
292 were available to be used in this study. For this part of the study, the ARMON was used as reference
293 being the only direct radon monitor running at both sites.

294 **3 Results**

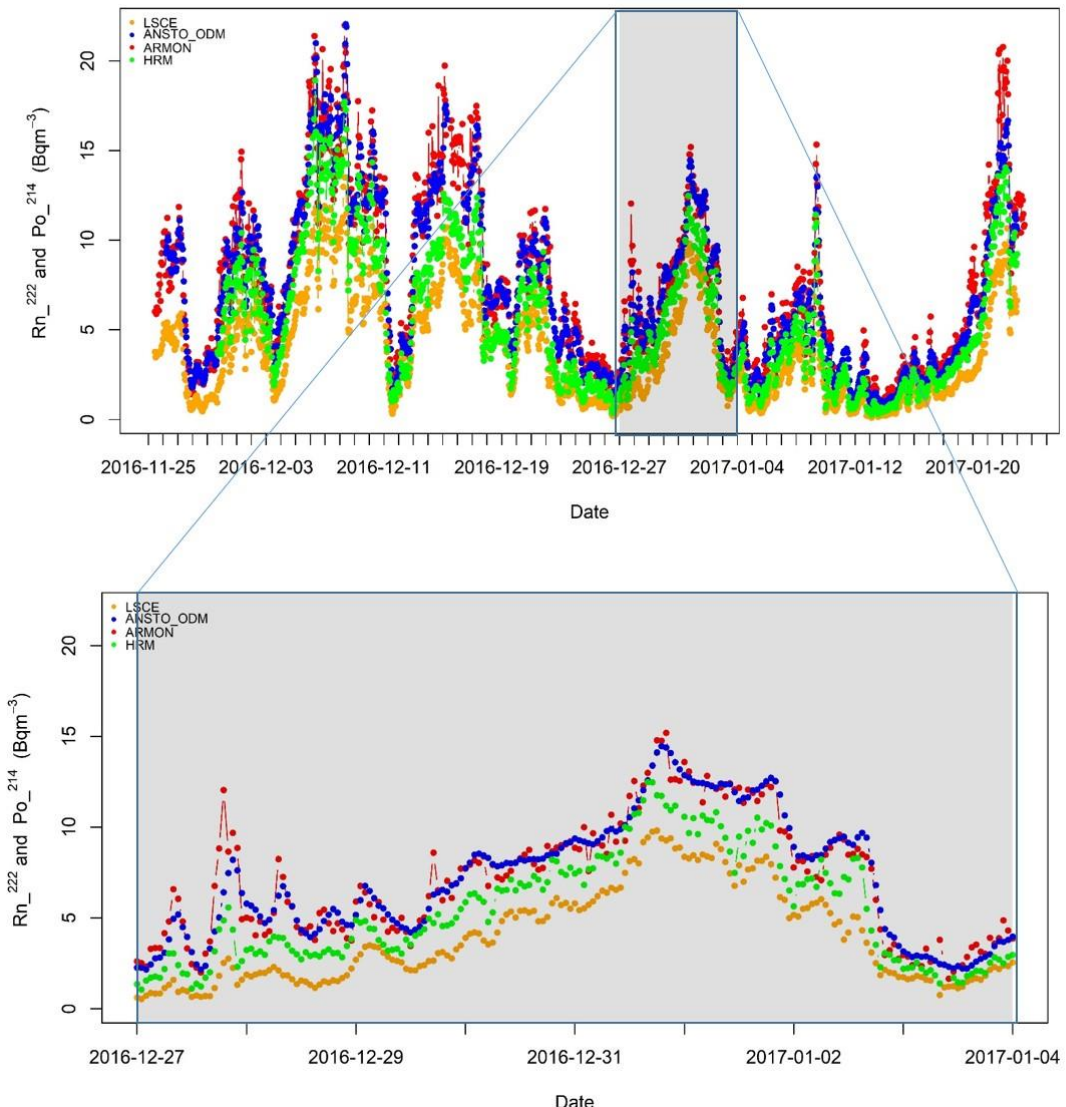
295 Hourly time serie s of atmospheric ^{222}Rn , in the case of ARMON and ANSTO monitors, and ^{222}Rn
296 progeny (^{214}Po activity concentration) for the HRM and LSCE monitors, measured at ODM and SAC
297 during Phase I and Phase II of the inter-comparison experiment are presented in Figures 2 and 3,
298 respectively. In each of the previous Figures, a zoom plot has been also reported as example to look at the
299 response of each monitor to the sub-diurnal atmospheric radon variability. As shown, all monitors
300 running at both sites follow this variability, with ^{222}Rn and ^{222}Rn progeny data measured or estimated by

301 the three different measurement techniques showing the same general patterns. Table 2 summaries the
302 means, minima and maxima hourly atmospheric radon or radon progeny activity concentrations measured
303 by each monitor for both campaigns. For further information, Figures S1 and S2 of the supplementary
304 material show the time series of the differences (absolute) and of the ratios (relative) between the hourly
305 ^{214}Po or ^{222}Rn activity concentrations measured by HRM, LSCE and ANSTO monitors and those
306 measured by the ARMON.

307 **3.1 Phase I: ODM site**

308 During Phase I the LSCE, HRM, ARMON and ANSTO_ODM monitors were operating in parallel,
309 sampling air from the same height (2 m a.g.l.). The mean temperature over Phase I of the campaign was
310 2.9 °C with an interquartile range of 0.10 °C to 5.8 °C. The mean relative humidity was 80% with an
311 interquartile range of 73% to 89%. An average accumulated rain per day of 13 mm was recorded. The
312 main wind patterns during Phase I were from northeast and southwest, with speeds typically between 1
313 and 7 m s⁻¹. The mean atmospheric aerosol concentration observed at ODM during Phase I was 505
314 particles cm⁻³ with an interquartile range of 233 cm⁻³ to 660 cm⁻³.

315 The means of the atmospheric ^{222}Rn activity concentration measured by the ARMON and the
316 ANSTO_ODM are in the same order (Table 2). The means of the atmospheric ^{214}Po activity
317 concentrations measured by LSCE monitor were ca. 50% lower and by the HRM ca. 30% lower than the
318 atmospheric ^{222}Rn activity concentration.



319

320

321 Figure 2. Main panel: Hourly time series of the atmospheric ^{222}Rn and, in the case of LSCE and HRM
 322 data ^{214}Po activity concentration, measured at Orme de Merisiers (ODM) station during Phase I (between
 323 25 November 2016 and 23 January 2017) by: ARMON (red circles), ANSTO_ODM (blue circles), HRM
 324 (green circles) and LSCE (orange circles) monitors. Zoomed panel: Hourly time series of the atmospheric
 325 ^{222}Rn and ^{214}Po measured between 27th December 2016 and 04th January 2017.

326 Table 2 shows the slopes (b) and intercepts (a) of the linear regression fits calculated between the hourly
 327 atmospheric ^{222}Rn and ^{214}Po activity concentrations measured by the ARMON and/or the HRM and the
 328 other ^{222}Rn and ^{222}Rn progeny monitors deployed in Phase I. The calculated slopes were in the range of
 329 0.62 to 1.17 and the R^2 values varied between 0.90 and 0.96. The slope closest to unity was calculated
 330 between the ARMON and ANSTO_ODM monitors, and was 0.96 ± 0.01 , while the lowest slope was
 331 observed between the ARMON and LSCE monitors, and was 0.62 ± 0.01 . The highest correlation
 332 ($R^2=0.96$) was found between the HRM and LSCE monitors. The plots of the linear regression fits of the
 333 Phase I are shown in the left panels of the Figures S3, S4 and S5 of the supplementary material. Notably,

334 the offset (a value) of the regression between the ANSTO and ARMON detectors at ODM is considerably
 335 greater than that at SAC. The regression slopes are also slightly different. These differences are likely
 336 related to the limited calibration and background information available for the ANSTO_ODM detector for
 337 this inter-comparison project. In particular, a substantial component of the instrumental background
 338 signal is site specific. This is likely responsible for much of the change in offset value.

				x					
	Monitors Phase I	Mean (Bq m ⁻³)	Min/Max (Bq m ⁻³)	b (ARMON)	a (ARMON)	R^2 (ARMON)	b (HRM)	a (HRM)	R^2 (HRM)
y	ANSTO_ODM	7.02	0.73/22.04	0.96±0.01	-0.23±0.03	0.94	1.17±0.01	0.63±0.03	0.93
	HRM	5.45	0.26/18.91	0.82±0.01	-0.71±0.03	0.93	-	-	-
	ARMON	7.55	0.50/21.98	-	-	-	-	-	-
	LSCE	3.84	0.10/14.93	0.62±0.01	-0.85±0.03	0.90	0.76±0.004	-0.29±0.03	0.96
	Monitors Phase II	Mean (Bq m ⁻³)	Min/Max (Bq m ⁻³)	Slope (ARMON)	Intercept (ARMON)	R^2 (ARMON)	Slope (HRM)	Intercept (HRM)	R^2 (HRM)
	ANSTO_SAC	3.50	0.43/10.71	0.97±0.01	0.01±0.06	0.95	1.03±0.01	0.15±0.06	0.90
	HRM	3.26	0.26/11.15	0.94±0.01	-0.13±0.06	0.91	-	-	-
	ARMON	3.60	0.17/11.51	-	-	-	-	-	-

339 Table 2. The means, maxima, and minima of the atmospheric ^{222}Rn and ^{214}Po activity concentration
 340 observed by each monitor participating in the Phase I and II of the inter-comparison campaigns. The
 341 slopes (b) and intercepts (a) of the linear regression fits calculated between the hourly atmospheric ^{222}Rn
 342 and ^{214}Po activity concentrations measured by the ARMON and/or the HRM and the other ^{222}Rn and
 343 ^{222}Rn progeny monitors deployed in both phases are also reported.

344 3.2 Phase II: SAC station

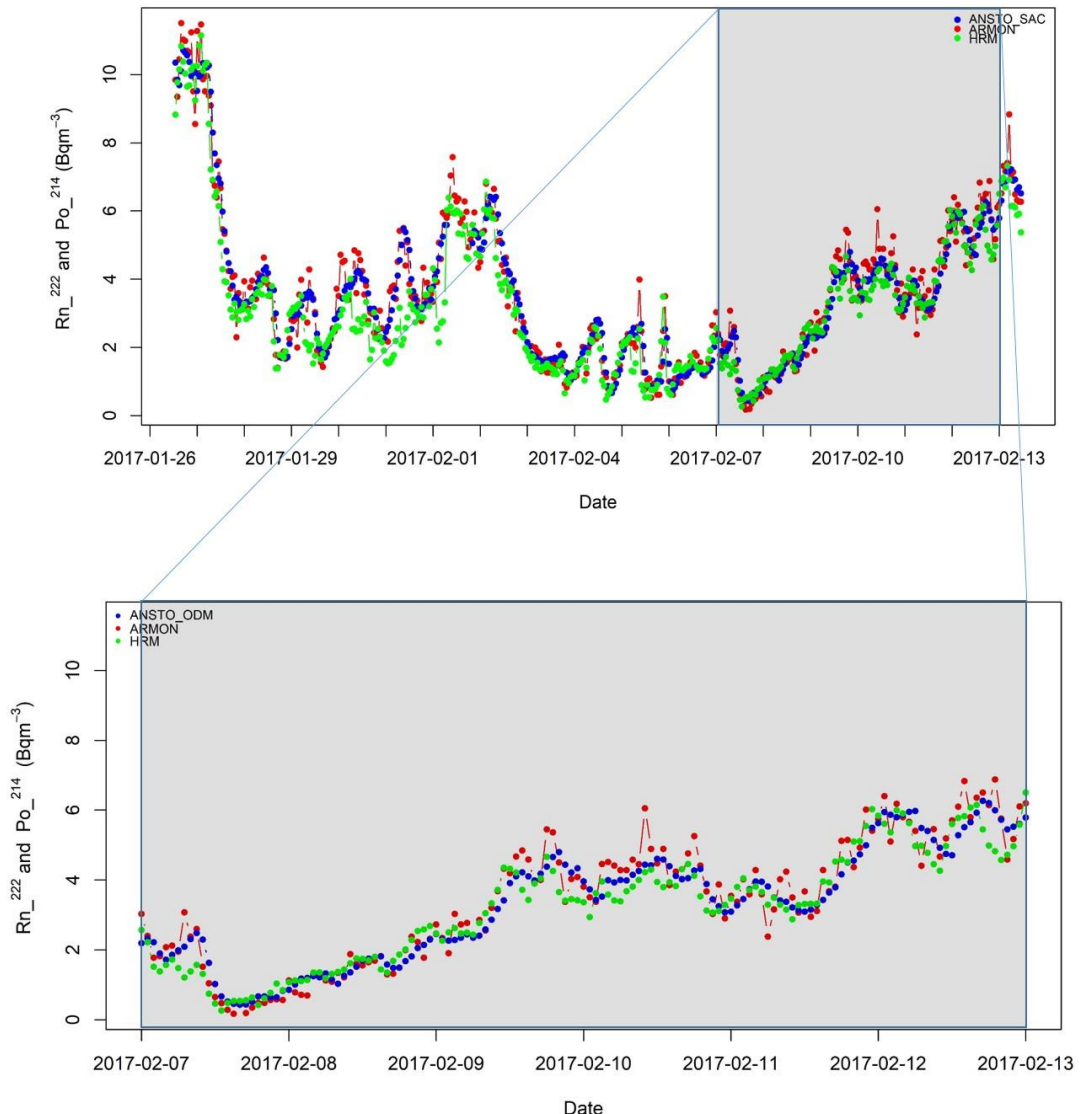
345 Phase II lasted 18 days. The mean temperature during this period was 5 °C with an interquartile range of 2
 346 °C to 8 °C. The mean relative humidity was 86% with an interquartile range of 80% to 94%. An average
 347 accumulated rain per day of 3 mm was recorded. The main wind patterns during this phase at 100 m a.g.l.
 348 were from the south and southwest with speeds typically between 3 and 10 m s⁻¹.

349 Figure 3 shows the hourly atmospheric ^{222}Rn and ^{214}Po activity concentrations observed at SAC during
 350 Phase II by the ARMON, HRM and ANSTO_SAC instruments.

351 Table 2 reports the means, minima, and maxima of the atmospheric data measured during Phase II by all
 352 participating monitors. In this case, the mean atmospheric ^{222}Rn and ^{214}Po activity concentrations
 353 measured by all monitors agreed within the instrumental errors. At 100 m a.g.l. the slopes of the hourly
 354 fits of the monitor's response in this case were all close to unity. The calculated offsets also decreased at
 355 100 m a.g.l. relative to 2 m a.g.l. The plots of the linear regression fits of Phase II are shown in the right
 356 panel of Figures S5 and S6 of the supplementary material. During the period of Jan 30 – February 1,
 357 2019, the HRM shows significantly lower values than the ANSTO and ARMON. This period coincides
 358 with saturated air humidity conditions.

359 Figure S7 of the supplementary material presents two plots to summarize the results of the slopes and
 360 offsets calculated both at ODM and SAC stations relative to the ARMON.

361



362

363 Figure 3. Main panel: Hourly time series of the atmospheric ^{222}Rn and ^{214}Po (HRM) activity concentration
 364 measured at Saclay (SAC) station between 25 January 2017 and 13 February 2017 by: ARMON (red
 365 circles), ANSTO_SAC (blue circles) and HRM (green circles) monitors. Zoomed panel: Hourly time
 366 series of the atmospheric ^{222}Rn and ^{214}Po measured between 7 February 2017 and 13 February 2017.

367 Figure 2 and 3 show a larger hourly variability of the HRM and ARMON signals compared with the
 368 ANSTO ones. This difference in variability is likely due to a larger uncertainty of the HRM and
 369 ARMON detectors and that only an approximated form of the Griffiths et al. (2016) response time
 370 correction could be applied to the output of the ANSTO detectors at these sites due to the incomplete
 371 calibration information. Further investigations should be carried out to clarify these differences and to
 372 exactly quantify the detectors uncertainties for the low ^{222}Rn concentrations typical for outdoor
 373 environmental monitoring at or above 100 m a.g.l.

374 **3.2 Comparison with past studies**

375 The results obtained in the present study of the slopes (b) and of the offsets (a) of the regression lines
 376 calculated between ANSTO or LSCE monitors against the HRM are here compared with the ones
 377 presented by Schmithüsen et. al., 2017. Table 3 shows a summary of this comparison. All slopes
 378 (correction factors) are defined as (routine station monitor) / HRM because this last was used as reference
 379 instrument by Schmithüsen et. al., 2017.

Site/Input Height	Schmithüsen et al., 2017			Present study		
ANSTO/HRM	Activity Range (Bq m ⁻³)	b	a	Activity Range (Bq m ⁻³)	b	a
Cabauw: 200/180 m	0-8	1.11±0.04	0.11±0.06			
Saclay: 100 m				0-11	1.03±0.01	0.15±0.06
Lutjewad: 60 m	0-6	1.11 ± 0.02	0.11 ± 0.02			
Heidelberg: 35 m	0-15	1.22 ± 0.01	0.42 ± 0.04			
Cabauw: 20 m	0-12	1.30 ± 0.01	0.21 ± 0.03			
Orme des Mérissiers: 2 m				0-22	1.17±0.01	0.63±0.03
LSCE/HRM	Activity Range (Bq m ⁻³)	b	a	Activity Range (Bq m ⁻³)	b	a
Orme des Mérissiers: 2 m	0-9	0.68±0.03	-0.18±0.09	0-15	0.76±0.01	-0.29±0.03

380 Table 3. Offsets and slopes of the regression lines calculated between ANSTO or LSCE monitors against
 381 the HRM in the present study and by Schmithüsen et. al., 2017.

382 Data in Table 3 need to be analysed taking into account that a unique traceability chain is not yet
 383 available for atmospheric radon measurements and the different monitors routinely running at the
 384 different stations could have different calibration chains (e.g. radon source, primary standard, etc.).
 385 Generally speaking, for both studies, it can be observed that the correction factor between the atmospheric
 386 ²¹⁴Po activity concentration measured by HRM and the atmospheric ²²²Rn activity concentration
 387 measured by ANSTO at each station approaches unity with the increase of the height of the sampling
 388 input. By contrast, the offsets of the regression fits decrease with the increase of the input height.

389 The only case where the compared instruments were exactly the same and at the same height is for Orme
 390 des Mérissiers station. Here the slope between the atmospheric ²¹⁴Po activity concentration measured by
 391 LSCE and HRM is equal to 0.76±0.01. This number is slightly larger but within uncertainties well
 392 comparable to the number reported by Schmithüsen et al. (2017) of 0.68±0.03 (see Table 3).

393

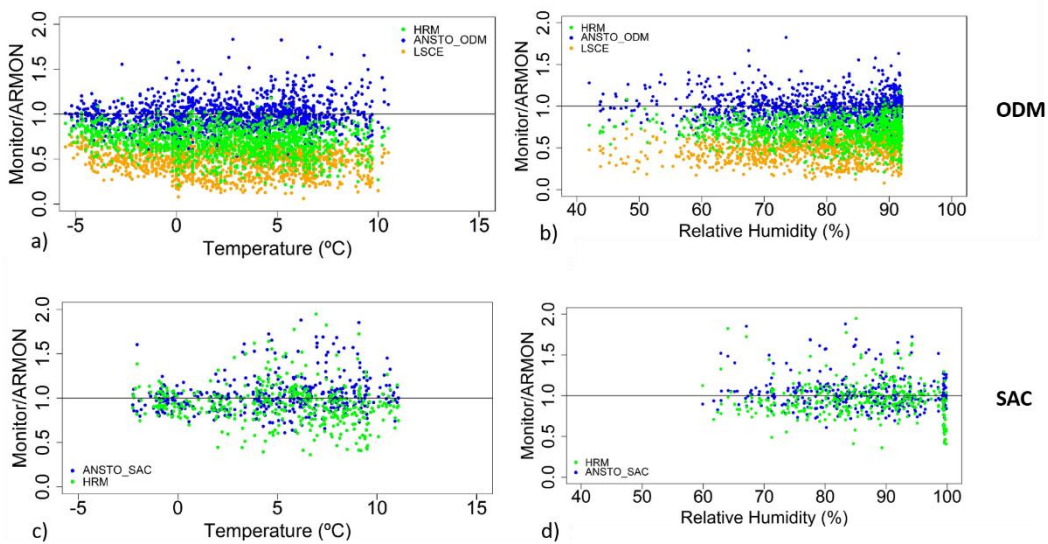
394 3.4 Influence of the weather conditions on the ratio between ²¹⁴Po and ²²²Rn measurements

395 Figure 4 shows the variability of the ratio between hourly atmospheric ²¹⁴Po and/or ²²²Rn activity
 396 concentration measured by each monitor relative to those measured by the ARMON versus the hourly
 397 means of ambient temperature and relative humidity. Analysis was carried out at ODM (Figure 4, upper
 398 panels) and at SAC (Figure 4, bottom panels) versus ambient temperature (Figures 4, left panels) and
 399 relative humidity (Figures 4, right panels) measured at the corresponding stations.

400 Figure 5 shows the same variability plotted in relation to the ANSTO_ODM at ODM (Figure 5, upper
 401 panels) and to the ANSTO_SAC at SAC (Figure 5, bottom panels) versus the hourly means of ambient
 402 temperature (Figures 5, left panels) and relative humidity (Figures 5, right panels).

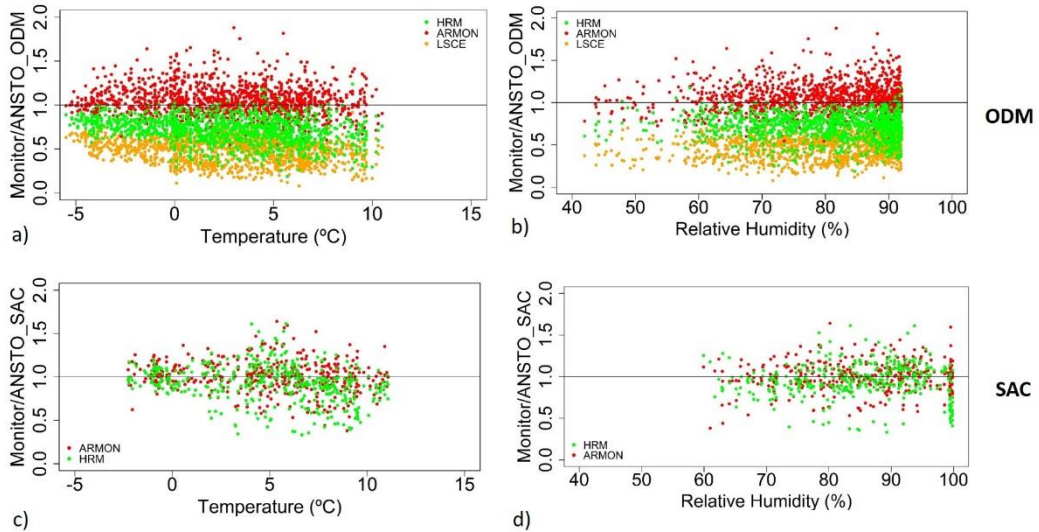
403 Data does not show any evident patterns at 100 m a.g.l. (SAC station), which could indicate that there is
 404 any impact on ²²²Rn or ²²²Rn progeny measurements due to change of ambient temperature and relative
 405 humidity, at least not until saturated conditions are achieved. By contrast, a small decrease, of about 10⁻²

406 $^{\circ}\text{C}^{-1}$, is observed in the ratio between the ^{214}Po activity concentration (measured by HRM and LSCE monitors) and the ^{222}Rn activity concentration (measured by ANSTO_ODM and ARMON monitors) with the increase of the ambient temperature (Figure S8 of the supplementary material) at 2 m a.g.l. (ODM station). This temperature dependency may be rather due to the effect of atmospheric activity concentrations, increasing during nighttime, on the disequilibrium between radon and its progeny. 409
 410 However, this influence on measured $^{214}\text{Po}/^{222}\text{Rn}$ ratios is really small compared with others observed 411 effects (e.g.: loss of progeny within the sample tube (Levin et al., (2017)), atmospheric aerosol 412 concentration (see below)). Looking at Figure 5, there appears to be less scatter in the point clouds 413 (particularly at SAC) when the ANSTO_SAC monitor is used as the reference, likely attributable to the 414 lower measurement uncertainty of the ANSTO monitor used at this station. 415



416

417 Figure 4. Hourly atmospheric ^{222}Rn or ^{214}Po activity concentration obtained by HRM, LSCE and ANSTO 418 monitors divided by the ^{222}Rn activity concentration measured by the ARMON detector as function of the 419 hourly measured atmospheric temperature and relative humidity at ODM (a and b) and at SAC (c and d), 420 respectively.



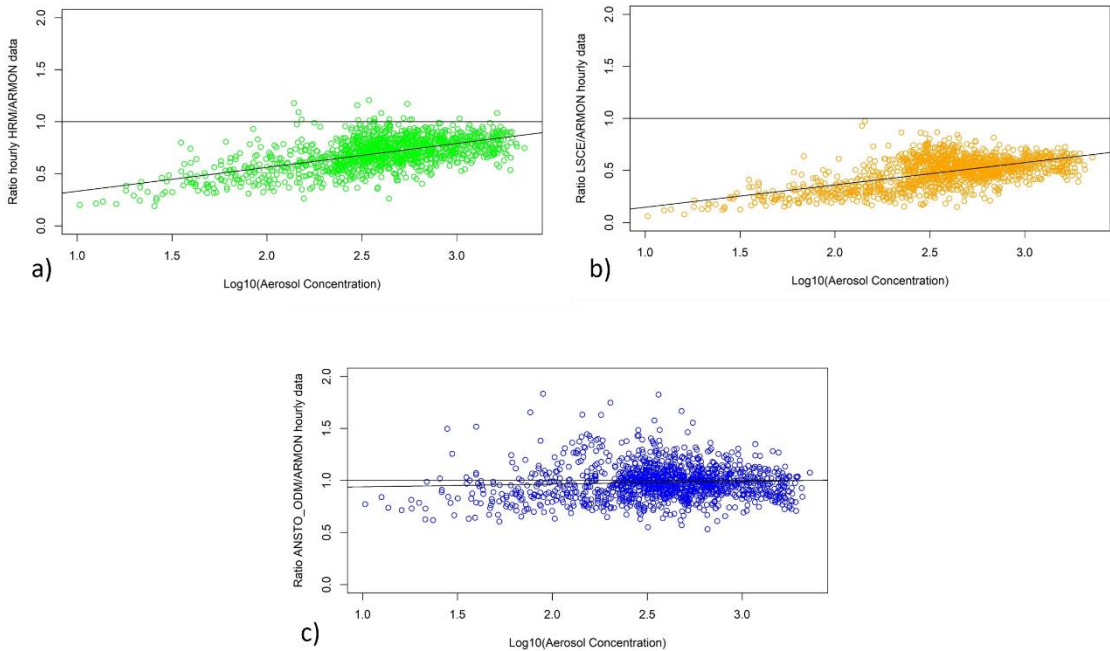
421

422 Figure 5. Hourly atmospheric ^{222}Rn or ^{214}Po activity concentration obtained by ARMON, HRM and
 423 LSCE monitors divided by the ^{222}Rn activity concentration measured by the ANSTO detectors as function
 424 of the hourly measured atmospheric temperature and relative humidity at ODM (a and b) and at SAC (c
 425 and d), respectively.

426 In Figure 6 the ratio of the hourly atmospheric ^{222}Rn or ^{222}Rn progeny activity concentration measured by
 427 the HRM (^{214}Po in Figure 6a), the LSCE (^{214}Po in Figure 6b) and the ANSTO_ODM (^{222}Rn in Figure 6c)
 428 monitor and the ^{222}Rn activity concentration measured with ARMON (^{222}Rn) are plotted against the
 429 logarithm of the hourly aerosol concentration data. Data indicate the existence of a linear relationship
 430 between these variables, i.e. of the form:

431
$$\frac{^{222}\text{Rn}(\text{Monitor}_i)}{^{222}\text{Rn}(\text{ARMON})} = a + b \cdot \log_{10}(\text{Aerosol Conc.}) \quad (1)$$

432 Here $^{222}\text{Rn}(\text{Monitor}_i)$ is the hourly atmospheric ^{222}Rn or ^{214}Po activity concentration measured by
 433 individual monitors HRM (^{214}Po), LSCE (^{214}Po) and ANSTO_ODM (^{222}Rn), $^{222}\text{Rn}(\text{ARMON})$ is the one
 434 measured by the ARMON monitor and *Aerosol Conc.* is the hourly atmospheric aerosol concentration
 435 measured at ODM during Phase I. The results of the linear regression fits are reported in Table 4. The
 436 slope of the ratio between the ANSTO_ODM and ARMON monitors in relation to the variability of the
 437 logarithm of the hourly atmospheric aerosol concentration is close to zero and the intercept is close to
 438 one. The ratio between the hourly atmospheric aerosol-bound radon progeny data measured by the two
 439 one-filter radon progeny monitors and the one measured by the ARMON seems to decrease with
 440 decreasing aerosol concentration (Figures 6a and 6b). However, this effect becomes only evident when
 441 atmospheric aerosol concentration is lower than $300 \text{ particles cm}^{-3}$.



442

443 Figure 6. Ratio of the atmospheric ^{222}Rn or ^{214}Po activity concentration measured by the HRM (green
 444 dots), LSCE (orange dots) and ANSTO_ODM (blue dots) monitors and those measured by the reference
 445 ARMON monitor against the logarithm of the atmospheric aerosol concentration measured at ODM
 446 station.

447 Table 4. Intercepts and slopes of the linear regression fits of the Equation 1

448 **Conclusions**

449 In order to confirm and build upon the results obtained by Xia et al. (2010), Grossi et al. (2016) and
 450 Schmithüsen et al. (2017) a three month inter-comparison campaign was carried out in the south of Paris,
 451 France, in the fall-winter period of 2016-2017. For the first time, three fundamentally distinct radon and
 452 radon progeny measurement approaches were compared side-by-side at two measurement heights: 2 and
 453 100 m a.g.l., under a range of environmental conditions with the aim to compare their responses.

454 The results of this study show that ^{222}Rn and ^{222}Rn progeny measurements follow the same general
 455 patterns of diurnal variability, both close to and further up from the surface. The slopes and intercepts of
 456 the linear regression fits between the radon and the radon-progeny measurements, which represent the
 457 calibration factors, are not significantly different from one at 100m height above ground (SAC), but they
 458 differ at the 2m level (ODM). This last behavior is attributable to the disequilibrium known to exist
 459 between ^{222}Rn freshly emitted from the ground and its short-lived progeny in the lowest 10s of meters of
 460 the atmosphere, the magnitude of which is known to decrease with distance from the surface, as shown in
 461 earlier work, and to be close to one at a height of 100m and above (e.g. Jacobi and André, 1963;
 462 Schmithüsen et al., 2017).

463 For the 2 m level, we found a very good correlation of radon progeny activity concentrations between
464 LSCE and HRM measurements (see Figure S3 in the Supplement). The slope, however, is only equal to
465 0.76 ± 0.01 . This number is slightly larger but within uncertainties well comparable to the number reported
466 by Schmithüsen et al. (2017) of 0.68 ± 0.03 (see Table 3) based on a comparison campaign conducted at
467 ODM in March and April 2014.

468 Observations of the total atmospheric aerosol concentration available at ODM station during the first two
469 months of the experiment were used to investigate the influence of changing atmospheric aerosol
470 concentrations on the response of the radon/progeny measurements. Under very low atmospheric
471 aerosol loading (< 300 particles cm^{-3}), the ^{222}Rn progeny monitors seem to underestimate the atmospheric
472 ^{214}Po activity concentrations by up to 50%. This effect may be attributable to loss of un-attached ^{218}Po
473 and ^{214}Po . Particle number concentrations below 300 particles cm^{-3} at continental stations are, however,
474 very rare and even during winter at Alpine stations like Schneefernerhaus such low particle
475 concentrations are only occasionally observed (Birmili et al., 2009).

476 The comparison of the results obtained in the present study with the ones reported in Schmithüsen et al.
477 (2017) underlines that to assure the harmonization of the atmospheric ^{222}Rn activity concentrations
478 measured at atmospheric networks is important to: i) have a well-established metrological chain; ii) use as
479 mobile reference instrument a direct radon monitor which response is not influenced by meteorological
480 conditions or inlet tube dimensions and length.

481 Finally, the new portable ARMON seems to have a great potential for being used within atmospheric
482 radon networks. In order to deeply evaluate the qualities and faults of this new instrument a long term
483 inter-comparison study should be carried out using a direct ANSTO instrument.

484 **Acknowledgments**

485 The research leading to these results has received funding from the Ministerio Español de Economía y
486 Competitividad, Retos 2013 (2014–2016) with the MIP (Methane interchange between soil and air over the
487 Iberian Península) project (reference: CGL2013-46186-R). This study was carried out under the umbrella
488 of the Atmospheric Thematic Center (ATC) of ICOS.

489 Claudia Grossi particularly thanks the Ministerio Español de Educación, Cultura y Deporte, for partially
490 supporting her work with the research mobility grant “José Castillejos” (ref. CA15/00042).

491 The authors warmly thank (i) the INTE team, in the persons of Vicente Blasco and Juan Antonio Romero,
492 for their work in the building of the ARMON used in this study; (ii) the R project (www.r-project.org)
493 free software environment used here for statistical computing and graphics.

494 This paper is dedicated to: Bruno Grossi, Dr. Manuel Javier Navarro Angulo, Dr. Alfredo Adán and the
495 whole team of the Instituto Clínic de Oftalmología (ICOF) of the Hospital Clínic of Barcelona.

496 **References**

497 Baskaran, M.: Po-210 and Pb-210 as atmospheric tracers and global atmospheric Pb-210 fallout: a
498 Review. J. of Environ. Radioact. 102 (5), 500-513, doi: 10.1016/j.jenvrad.2010.10.007, 2010.

499 Baskaran, M.: Radon: A Tracer for Geological, Geophysical and Geochemical Studies" Springer
500 Geochemistry book series (SPRIGEO), 2016.

501 Biraud, S.: Vers la régionalisation des puits et sources des composés à effet de serre: analyse de la
502 variabilité synoptique à l'observatoire de Mace Head, Irlande, PhD Thesis, University of Paris VII,
503 France, 2000.

504 Birmili, W., L. Ries, R. Sohmer, A. Anastou, A. Sonntag, K. Konig, I. Levin, 2009b. Fine and ultrafine
505 aerosol particles at the GAW station Schneefernerhaus/Zugspitze. – Gefahrst. Reinh. Luft 69(1/2), 31–35.

506 Chambers, S. D., A. G. Williams, W. Zahorowski, A. Griffiths, and J. Crawford: Separating remote fetch
507 and local mixing influences on vertical radon measurements in the lower atmosphere. Tellus B, 63(5),
508 843-859, doi: 10.1111/j.1600-0889.2011.00565.x, 2011.

509 Chambers, S. D., W. Zahorowski, A. G. Williams, J. Crawford, and A. D. Griffiths: Identifying
510 tropospheric baseline air masses at Mauna Loa Observatory between 2004 and 2010 using Radon-222 and
511 back trajectories, J. Geophys. Res.: Atmos., 118(2), 992-1004, doi: 10.1029/2012JD018212, 2013.

512 Chambers, S. D., S. B. Hong, A. G. Williams, J. Crawford, A. D. Griffiths, and S. J. Park: Characterising
513 terrestrial influences on Antarctic air masses using Radon-222 measurements at King George Island,
514 Atmos. Chem. Phys., 14, 9903-9916, doi:10.5194/acp-14-9903-2014, 2014.

515 Chambers, S. D., A. G. Williams, F. Conen, A. D. Griffiths, S. Reimann, M. Steinbacher, P. B. Krummel,
516 L. P. Steele, M. V. van der Schoot, I. E. Galbally, S. B. Molloy, and J. E. Barnes: Towards a universal
517 "baseline" characterisation of air masses for high- and low-altitude observing stations using Radon-222,
518 Aerosol Air Qual. Res., 16, 885-899, doi: 10.4209/aaqr.2015.06.0391, 2015.

519 Chambers, S.D. D. Galeriu, A.G. Williams, A. Melintescu, A.D. Griffiths, J. Crawford, L. Dyer, M.
520 Duma, B. Zorila: Atmospheric stability effects on potential radiological releases at a nuclear research
521 facility in Romania: Characterising the atmospheric mixing state. J. of Environ. Radioact., 154, 68-82,
522 doi: 10.1016/j.jenvrad.2016.01.010, 2016.

523 Chambers SD, Preunkert S, Weller R, Hong S-B, Humphries RS, Tositti L, Angot H, Legrand M,
524 Williams AG, Griffiths AD, Crawford J, Simmons J, Choi TJ, Krummel PB, Molloy S, Loh Z, Galbally I,
525 Wilson S, Magand O, Sprovieri F, Pirrone N and Dommergue A.: Characterizing Atmospheric Transport
526 Pathways to Antarctica and the Remote Southern Ocean Using Radon-222, Front. Earth Sci., 6:190,
527 https://doi.org/10.3389/feart.2018.00190, 2018.

528 Chambers SD, Guérette E-A, Monk K, Griffiths AD, Zhang Y, Duc H, Cope M, Emmerson KM, Chang
529 LT, Silver JD, Utembe S, Crawford J, Williams AG and Keywood M.: Skill-testing chemical transport
530 models across contrasting atmospheric mixing states using Radon-222, Atmosphere 10 (1), 25;
531 https://doi.org/10.3390/atmos10010025, 2019a

532 Chambers SD, Podstawczyńska A, Pawlak W, Fortuniak K, Williams AG and Griffiths AD.:
533 Characterising the state of the urban surface layer using Radon-222, J. Geophys. Res. Atmos., 124(2),
534 770-788, https://doi.org/10.1029/2018JD029507, 2019b.

535 Frank, G., Salvamoser, J., and Steinkopf, T.: Messung radioaktiver Spurenstoffe in der Atmosphäre im
536 Rahmen des Global Atmosphere Watch Programmes der WMO, Umweltforschungsstation
537 Schneefernerhaus, Wissenschaftliche Resultate 2011/2012,
538 http://www.schneefernerhaus.de/fileadmin/web_data/bilder/pdf/UFS-Broschuere_2012.pdf, last access:
539 18 August, 2016.

540 Galmarini, S.: One year of ^{222}Rn concentration in the atmospheric surface layer, *Atmos. Chem. Phys.*, 6,
541 2865-2887, doi: 10.5194/acp-6-2865-2006, 2006.

542 Griffiths, A. D., Chambers, S. D., Williams, A. G., and Werczynski, S.: Increasing the accuracy and
543 temporal resolution of two filters radon-222 measurements by correcting for the instrument response,
544 *Atmos. Meas. Tech.*, 9, 2689–2707, doi:10.5194/amt-9-2689-2016, 2016.

545 Grossi, C., Arnold, D., Adame, A. J., Lopez-Coto, I., Bolivar, J. P., de la Morena, B. A., and Vargas, A.:
546 Atmospheric ^{222}Rn concentration and source term at El Arenosillo 100m meteorological tower in
547 southwest, Spain. *Radiat. Meas.*, 47, 149–162, doi:10.1016/j.radmeas.2011.11.006, 2012.

548 Grossi, C., Àgueda, A., Vogel, F. R., Vargas, A., Zimnoch, M., Wach, P., Martín, J. E., López-Coto, I.,
549 Bolívar, J. P., Morguí, J.-A., and Rodó, X.: Analysis of ground-based ^{222}Rn measurements over Spain:
550 filling the gap in southwestern Europe, *J. Geophys. Res.-Atmos.*, 121, 11021–11037,
551 <https://doi.org/10.1002/2016JD025196>, 2016.

552 Grossi, C., Vogel, F. R., Curcoll, R., Àgueda, A., Vargas, A., Rodó, X., and Morguí, J.-A.: Study of the
553 daily and seasonal atmospheric CH_4 mixing ratio variability in a rural Spanish region using ^{222}Rn tracer,
554 *Atmos. Chem. Phys.*, 18, 5847-5860, <https://doi.org/10.5194/acp-18-5847-2018>, 2018.

555 Gutiérrez-Álvarez, I. Guerrero, J. L. Martín, J. E. Adame, J. A. Vargas, A. Bolívar, J. P.: Radon behavior
556 investigation based on cluster analysis and atmospheric modelling, *Atm. Environ.* 201, 50-61, doi:
557 10.1016/j.atmosenv.2018.12.010, 2019.

558 Hernández-Ceballos, M. A., A. Vargas, D. Arnold, and J. P. Bolívar: The role of mesoscale meteorology
559 in modulating the ^{222}Rn concentrations in Huelva (Spain) - impact of phosphogypsum piles, *J. Environ.*
560 *Radioact.*, 145, 1-9, doi: 10.1016/j.jenvrad.2015.03.023, 2015.

561 Hirao, S., H. Yamazawa, and J. Moriizumi: Inverse modelling of Asian ^{222}Rn flux using surface air
562 ^{222}Rn concentration, *J. Environ. Radioact.*, 101(11), 974-984, doi: 10.1016/j.jenvrad.2010.07.004, 2010.

563 Hopke, P. K.: The initial behavior of ^{218}Po in indoor air. *Environment International*, 15, 299-308, 1989.

564 Jacobi, W. and André, K.: The vertical distribution of Radon 222, Radon 220 and their decay
565 products in the atmosphere, *J. Geophys. Res.*, 68, 3799–3814, 1963.

566 IAEA (International Atomic Energy Agency): Sources and Measurements of Radon and Radon Progeny
567 Applied to Climate and Air Quality Studies. Proceedings of a technical meeting held in Vienna, organized
568 by the International Atomic Energy Agency and co-sponsored by the World Meteorological Organization,
569 IAEA, Austria, Vienna, 2012.

570 Krystek, M. and Anton, M. 2007. A weighted total least-squares algorithm for fitting a straight line.
571 Meas. Sci. Technol. 18, 3438–3442, doi:10.1088/0957-0233/18/11/025

572 Levin, I., H. Glatzel-Mattheier, T. Marik, M. Cuntz, M. Schmidt, and D. E. J. Worthy: Verification of
573 German methane emission inventories and their recent changes based on atmospheric observations, J.
574 Geophys. Res., 104(D3), 3447-3456, doi: 10.1029/1998JD100064, 1999.

575 Levin, I., Hammer, S., Eichelmann, E. and Vogel, F.R.: Verification of greenhouse gas emission
576 reductions: the prospect of atmospheric monitoring in polluted areas. Philosophical Transactions of the
577 Royal Society of London A: Mathematical, Physical and Engineering Sciences, 369(1943), 1906-1924,
578 2011

579 Levin, I., Born, M., Cuntz, M., Langendörfer, U., Mantsch, S., Naegler, T., Schmidt, M., Varlagin, A.,
580 Verclas, S., and Wagenbach, D.: Observations of atmospheric variability and soil exhalation rate of
581 Radon-222 at a Russian forest site: Technical approach and deployment for boundary layer studies, Tellus
582 B, 54, 462–475, 2002.

583 Levin, I., Schmithüsen, D., and Vermeulen, A.: Assessment of 222radon progeny loss in long tubing
584 based on static filter measurements in the laboratory and in the field, Atmos. Meas. Tech., 10, 1313–1321,
585 doi:10.5194/amt-10-1313-2017, 2017.

586 Locatelli, R., P. Bousquet, F. Hourdin, M. Saunois, A. Cozic, F. Couvreux, J. Y. Grandpeix, M. P.
587 Lefebvre, C. Rio, P. Bergamaschi, S. D. Chambers, U. Karstens, V. Kazan, S. van der Laan, H. A. J.
588 Meijer, J. Moncrieff, M. Ramonet, H. A. Scheeren, C. Schlosser, M. Schmidt, A. Vermeulen, and A. G.
589 Williams: Atmospheric transport and chemistry of trace gases in LMDz5B: evaluation and implications
590 for inverse modelling, Geosci. Model Dev., 8, 129–150, doi: 10.5194/gmd-8-129-2015, 2015.

591 López-Coto, I., Mas, J.L., Bolívar, J.P.: A 40-year retrospective European radon flux inventory including
592 climatological variability, Atmos. Environ., 73, 22–33, doi: 10.1016/j.atmosenv.2013.02.043, 2013.

593 Nazaroff, W.W., and Nero, A.V. (Eds.): Radon and its decay products in indoor air, John Wiley & Sons,
594 New York, USA, doi: 10.1063/1.2810982, 1988.

595 Karstens, U., Schwingshakl, C., Schmithüsen, D., and Levin, I.: A process-based 222radon flux map for
596 Europe and its comparison to long-term observations, Atmos. Chem. Phys., 15, 12845-12865,
597 <https://doi.org/10.5194/acp-15-12845-2015>, 2015.

598 Paatero, J., Hatakka, J., and Viisanen, Y.: Concurrent measurements of airborne radon-222, lead-210 and
599 beryllium-7 at the Pallas-Sodankylä GAW station, Northern Finland, Reports 1998:1, Finnish
600 Meteorological Institute, Helsinki, 1998.

601 Pereira, E.B. Pereira and da Silva, H. E.: Atmospheric radon measurements by electrostatic precipitation
602 Nucl. Instr. Methods, A280, 503–505, 1989.

603 Schery, S. D. and Huang, S.: An estimate of the global distribution of radon emissions from the ocean,
604 Geophys. Res. Lett., 31, L19104, doi:10.1029/2004GL021051, 2004.

605 Schmithüsen, D., Chambers, S., Fischer, B., Gilge, S., Hatakka, J., Kazan, V., Neubert, R., Paatero, J.,
606 Ramonet, M., Schlosser, C., Schmid, S., Vermeulen, A., and Levin, I.: A European wide 222radon and
607 222radon progeny comparison study, *Atmos. Meas. Tech.*, 10, 1299–1312, <https://doi.org/10.5194/amt-10-1299-2017>, 2017.

609 Stockburger, H. und Sittkus, A.: Unmittelbare Messung der natürlichen und künstlichen Radioaktivität
610 der atmosphärischen Luft, *Zeitschrift für Naturforschung*, 21, 1128–1132, 1966.

611 Szegvary, T., Conen, F. Ciais, P.: European 222Rn inventory for applied atmospheric studies, *Atmos.*
612 *Environ.*, 43(8), 1536–1539, doi: 10.1016/j.atmosenv.2008.11.025, 2009.

613 Tositti, L. Bueno Pereira, E. Sandrini, S. Capra, D. Tubertini, O. Bettoli, M. G.: Assessment of summer
614 trands of tropospheric radon isotopes in a costal antartic station (Terra Nova Bay). *Intern. J. Environ.*
615 *Anal. Chem.* 82, 5, 259–274, 2002

616 Vargas, A., D. Arnold, J. A. Adame, C. Grossi, M. A. Hernández-Ceballos, and J. P. Bolívar: Analysis of
617 the vertical radon structure at the Spanish “El Arenosillo” tower station, *J. Environ. Radioact.*, 139, 1-17,
618 doi: 10.1016/j.jenvrad.2014.09.018, 2015.

619 Vogel, F.R., M. Ishizawa, E. Chan, D. Chan, S. Hammer, I. Levin, and D. E. J. Worthy: Regional non-
620 CO₂ greenhouse gas fluxes inferred from atmospheric measurements in Ontario, Canada, *J. Integr.*
621 *Environ. Sci.*, 9 (S1), 1-15, doi: 10.1080/1943815X.2012.691884, 2012.

622 Vogel, F. R., B. Tiruchittampalam, J. Theloke, R. Kretschmer, C. Gerbig, S. Hammer, and I. Levin: Can
623 we evaluate a fine-grained emission model using high-resolution atmospheric transport modelling and
624 regional fossil fuel CO₂ observations?, *Tellus B*, 65, 18681, doi: 967
625 <http://dx.doi.org/10.3402/tellusb.v65i0.18681>, 2012.

626 Wada, A., H. Matsueda, S. Murayama, S. Taguchi, S. Hirao, H. Yamazawa, J. Moriizumi, K. Tsuboi, Y.
627 Niwa, and Y. Sawa: Quantification of emission estimates of CO₂, CH₄ and CO for East Asia derived
628 from atmospheric radon-222 measurements over the western North Pacific, *Tellus B*, 65, 18037, doi:
629 <http://dx.doi.org/10.3402/tellusb.v65i0.18037>, 2013.

630 Weller, R., Levin, I., Schmithüsen, D., Nachbar, M., Asseng, J., and Wagenbach, D. : On the variability
631 of atmospheric 222Rn activity concentrations measured at Neumayer, coastal Antarctica. *Atmos. Chem.*
632 *Phys.*, 14: 3843–3853, 2014.

633 Williams, A. G., W. Zahorowski, S. Chambers, A. Griffiths, J. M. Hacker, A: Element, and S.
634 Werczynski, S., The vertical distribution of radon in clear and cloudy daytime terrestrial boundary layers,
635 *J. Atmos. Sci.*, 68 (1), 155-174, doi: 10.1175/2010JAS3576.1, 2011.

636 Williams, A. G., S. Chambers, and A. Griffiths: Bulk mixing and decoupling of the nocturnal stable
637 boundary layer characterized using a ubiquitous natural tracer, *Boundary Layer Meteorol.*, 149(3), 381-
638 402, doi: 10.1007/s10546-013-9849-3, 2013.

639 Williams, AG and SD Chambers: A history of radon measurements at Cape Grim, Baseline Atmospheric
640 Program (Australia) History and Recollections (40th Anniversary Special Edition), 131-146, 2016.

641 Whittlestone, S., and W. Zahorowski: Baseline radon detectors for shipboard use: Development and
642 deployment in the First Aerosol Characterization Experiment (ACE 1), *J. Geophys. Res.*, 103(D13),
643 16743–16751, doi: 10.1029/98JD00687, 1998.

644 Xia, Y., H. Sartorius, C. Schlosser, U. Stöhlker, F. Conen, and W. Zahorowski: Comparison of one- and
645 two-filter detectors for atmospheric ^{222}Rn measurements under various meteorological conditions,
646 *Atmos. Meas. Tech.*, 3, 723-731, doi: 10.5194/amt-3-723-2010, 2010.

647 Zahorowski, W., S. D. Chambers, and A. Henderson-Sellers: Ground based radon-222 observations and
648 their application to atmospheric studies, *J. Environ. Radioact.*, 76(1-2), 3-33, doi:
649 10.1016/j.jenvrad.2004.03.033, 2004.

650 Zimnoch, M., P. Wach, L. Chmura, Z. Gorczyca, K. Rozanski, J. Godlowska, J. Mazur, K. Kozak, and A.
651 Jericevic: Factors controlling temporal variability of near-ground atmospheric ^{222}Rn concentration over
652 central Europe. *Atmos. Chem. Phys.* 14, 9567–9581, doi: 10.5194/acp-14-9567-2014, 2014.



Copernicus Publications

The Innovative Open Access Publisher

653

654

655